

This document is confidential and is proprietary to the American Chemical Society and its authors. Do not copy or disclose without written permission. If you have received this item in error, notify the sender and delete all copies.

**Reversible and quasireversible electron transfer under conditions of differential square-wave voltammetry**

Journal:	<i>The Journal of Physical Chemistry</i>
Manuscript ID	Draft
Manuscript Type:	Article
Date Submitted by the Author:	n/a
Complete List of Authors:	Guziejewski, Dariusz; Uniwersytet Lodzki, Department of Inorganic and Analytical Chemistry Stojanov, Leon; Ss Cyril and Methodius University in Skopje Institute of Chemistry, Gulaboski, Rubin; Univerzitet Goce Delcev Stip, Department of Chemistry Mirceski, Valentin; Uniwersytet Lodzki, Department of Inorganic and Analytical Chemistry; "SS Cyril and Methodius" University, Institute of Chemistry

SCHOLARONE™  
Manuscripts

---

# Reversible and quasireversible electron transfer under conditions of differential square-wave voltammetry

***Dariusz Guziejewski<sup>1</sup>, Leon Stojanov<sup>2</sup>, Rubin Gulaboski<sup>3</sup>,  
and Valentin Mirceski<sup>1,2\*</sup>***

*<sup>1</sup>Department of Inorganic and Analytical Chemistry, University of Lodz, Tamka 12, 91-403  
Lodz, Poland*

*<sup>2</sup>Institute of Chemistry, Faculty of Natural Sciences and Mathematics, P.O. Box 162, 1000  
Skopje, R. North Macedonia*

*<sup>3</sup>Faculty of Medical Sciences, Goce Delcev University, Stip, R. North Macedonia*

---

\* Corresponding author (valentin@pmf.ukim.mk)

## **Abstract**

A theoretical analysis of a reversible and quasireversible electrode reactions of a dissolved redox couple under conditions of the novel technique of differential square-wave voltammetry (DSWV) is presented. The technique is recently introduced as a hybrid form between differential pulse voltammetry (DPV) and square-wave voltammetry (SWV) as two most advanced and competitive pulse-form voltammetric techniques of, for a purpose of unifying their advantages and further advancing both techniques, in terms of analytical performances, mechanistic analysis, and electrode kinetics. The potential modulation of DSWV consists of potential steps and pulses providing a plethora of voltammetric curves which enable in-depth characterization of the electrode reaction with a minimal set of measurements. Based on numerical simulations a set of criteria for characterization and differentiation between reversible and quasireversible electrode reactions are established.

**Keywords:** Differential square-wave voltammetry, pulse voltammetry, electrode mechanism

## 1. Introduction

The last two decades or so are highlighted with a remarkable progress in voltammetry<sup>1-2</sup>, encompassing the advances in the theory of voltammetric techniques<sup>3-5</sup>, simulations of electrode mechanisms<sup>6-8</sup>, kinetics of electrode processes<sup>9-13</sup> and the novel type of pulse voltammetric techniques<sup>14</sup>. Pulse voltammetry is of distinct importance in the broad area of electro-analysis; moreover, pulse techniques are exceptionally important for studying electrode kinetics<sup>15-17</sup> and they aided significantly voltammetric studies of electron transfer theories<sup>18-20</sup>. The family of pulse voltammetric techniques has been constantly expanding with new techniques exemplified with differential double pulse voltammetry<sup>21</sup>, additive differential pulse voltammetry<sup>22</sup>, differential alternative pulses voltammetry<sup>23-25</sup>, cyclic multi-pulse voltammetry<sup>26</sup>, to mention just a few. Frequently, pulse techniques have been applied in a reverse mode<sup>27-28</sup> or in a cyclic fashion<sup>29-31</sup>, intending to unify their inherent advantages with conventional cyclic voltammetry. In the context of conventional cyclic voltammetry, as an inevitable technique in any electrochemical study, we do also witness a significant progress in the studies with non-triangular waveforms of Compton et al. aiming to circumvent the inherent drawbacks related with the charging current<sup>32-33</sup>. Moreover, the latter methodology introduces the concept of a single voltammetry experiment conducted with a range of scan rates, which might be an exciting direction for further advancing voltammetry in general. Accordingly, we have recently proposed a multi-frequency approach in a single experiment under conditions of electrochemical Faradaic spectroscopy<sup>34</sup>, which finds some analogy with a multi-scan rate analysis in the method of Compton et al<sup>33</sup>. Electrochemical Faradaic spectroscopy<sup>35</sup>, as a simple square-wave chronoamperometric experiment, has been derived from the conventional square-wave voltammetry (SWV)<sup>36-37</sup> in order to simplify the voltammetric analysis. It comes along with a series of new variants of SWV developed in the last decade<sup>29, 35, 38</sup>, as a quest for further advancing the technique.

In spite of the fact that SWV is one of the most advanced pulse techniques, it has been recognized that it is relatively complex, thus simplification and further modification are worth to be considered. For instance, SW voltammetric data are less intuitively understandable compared to cyclic voltammetry, rendering SWV predominantly as a tool in electro-analysis<sup>39-40</sup>. In the context of electrode kinetics SWV

is superior compared to other techniques when fast, reversible and quasireversible electrode processes are concerned; it is however limited when electrochemically sluggish processes are considered with a large potential separation between anodic and cathodic reactions of a single redox couple.

In order to advance further SWV we have recently made an attempt to develop its differential variant termed as differential square wave voltammetry (DSWV)<sup>41</sup>, proposing a new potential modulation which is more appropriate for kinetic analysis of both fast and sluggish electrode processes, while keeping the ability to study the electrode mechanism; in addition, the technique has a promising analytical performances being able to improve the response with respect to the background current discrimination in comparison with conventional SWV.

The potential modulation of DSWV, depicted in Fig. 1A, consists of a train of potential steps combined with potential pulses. A potential cycle of duration  $\tau_{\text{tot}}$  consists of a step potential ( $\tau_s$ ) followed by two, equal in heights, oppositely oriented potential pulses with duration  $t_p$  (Fig. 1B); thus,  $\tau_{\text{tot}} = \tau_s + 2t_p$ . The inverse value of  $2t_p$  is known as the SW frequency  $f$  ( $f = 1/(2t_p)$ ). Commonly,  $t_p$  ranges from 0.5 to 100 ms. In analogy to differential pulse voltammetry, the technique is characterized with a step-to pulse duration ratio  $r = \tau_s/t_p$ , which together with the SW frequency, is a critical parameter of the technique.

By measuring the current before the application of the pulses ( $I_s$ , in Fig. 1B), as well as at the end of each pulse ( $I_f$  and  $I_r$ , in Fig. 1B), both SW forward ( $I_f$ ) and reverse ( $I_r$ ) voltammetric components can be transformed into differential curves, designated as  $I_{f,\text{diff}} = I_f - I_s$  and  $I_{r,\text{diff}} = I_r - I_s$ , respectively. By analogy to SWV, net, differential voltammetric component can be constructed as well ( $I_{\text{net}} = I_f - I_r$ ). Finally, as proposed by Molina<sup>22</sup> an additive component can be constructed, i.e.,  $I_{\text{add}} = I_{f,\text{diff}} + I_{r,\text{diff}} = I_f + I_r - 2I_s$ . Thus, the voltammetric response can be represented by seven components, which provides a broad basis for in-depth electrochemical characterization.

Following the first introductory study<sup>41</sup>, in the current communication fundamental voltammetric characteristics of both reversible and quasireversible electrode reactions of a dissolved redox couple at a planar electrode are elucidated by means of numerical simulations. Theoretical predictions are partly illustrated by

experiments conducted with  $[\text{Fe}(\text{CN})_6]^{4-}/[\text{Fe}(\text{CN})_6]^{3-}$  redox couple at a platinum electrode (Pt) as a model for a fast electrode reaction of a dissolved redox couple<sup>42</sup>.

## 2. Details on electrode mechanisms and simulation procedure

A quasireversible one-electron electrode reaction is considered (eq. 1). The redox couple consists of two chemically stable species dissolved in an electrolyte solution (s) and the electrode reaction takes place at a macroscopic planar electrode.



For the sake of simplicity, the charge of the redox species in eq. (1) is omitted. At the beginning of the experiment only Red species are present in the solution at a bulk concentration of  $c_R^*$ . For the sake of simplicity, the diffusion coefficient ( $D$ ) of both Red and Ox is assumed to be equal. For a reversible electrode reaction Nernst equation holds:  $c(\text{Ox})_{x=0} = c(\text{Red})_{x=0} \exp(\phi)$ , where  $\phi = \frac{nF}{RT}(E - E^{\circ'})$  is the dimensionless electrode potential defined versus the formal potential of the redox couple ( $E^{\circ'}$ ). For a quasireversible one-electron reaction the electrode kinetics is described with a Butler-Volmer kinetic model, i.e.,  $\frac{I}{FA} = k_s \exp(\alpha\phi) [(c_{\text{Red}})_{x=0} - (c_{\text{Ox}})_{x=0} \exp(-\phi)]$  attributed with the standard rate constant  $k_s$  ( $\text{cm s}^{-1}$ ) and anodic electron transfer coefficient  $\alpha$ . Equations (2) and (3) were applied for the numerical simulation of a reversible and quasireversible electrode reaction, respectively, which were derived following the step function method<sup>43</sup>:

$$\psi_m = \frac{\sqrt{50\pi} \exp(\phi_m)}{2 [1 + \exp(\alpha\phi_m)]} - \sum_{j=1}^{m-1} \psi_j S_{m-j+1} \quad (2)$$

$$\psi_m = \frac{\kappa \exp(\alpha\phi_m) \left\{ 1 - \frac{2[1 + \exp(-\alpha\phi_m)]}{\sqrt{50\pi}} \sum_{j=1}^{m-1} \psi_j S_{m-j+1} \right\}}{1 + \frac{2\kappa \exp(\alpha\phi_m)}{\sqrt{50\pi}} [1 + \exp(-\alpha\phi_m)]} \quad (3).$$

The dimensionless current is defined as  $\psi = \frac{I}{FAc_R^* \sqrt{Df}}$ ,  $A$  is the electrode surface area,  $S_m = \sqrt{m} - \sqrt{m-1}$  is the numerical integration parameter, and  $m$  is the serial number of time increments. The time increment is  $d = \frac{1}{50f}$ , which means that each potential pulse is divided into 25 equal increments. Accordingly, the number of time increments

for the potential step  $\tau_s$  is  $25r$ , where  $r = \tau_s/t_p$  is the step-to pulse duration ratio. In addition,  $\kappa = \frac{k_s}{\sqrt{Df}}$  is the electrode kinetic parameter, and other symbols have their common meaning.

### 3. Experimental

All chemicals used were of analytical grade purity (Sigma-Aldrich, ChemLab or POCh). Aqueous solutions were prepared with deionized water with Millipore Direct Q-3 (Merck) purification system. Stock solutions of  $K_4[Fe(CN)_6]$ ,  $K_3[Fe(CN)_6]$  and  $KNO_3$  were prepared in water. In all experiments the electrolytic cell contained equimolar content of both forms of the redox couple at concentration of 0.25 mmol/L in 0.1 mol/L  $KNO_3$  used as a supporting electrolyte. All experiments were conducted at room temperature.

Experimental analysis has been performed with multi-Autolab potentiostat model M101 (Metrohm Autolab B.V.) controlled by the NOVA (v. 1.10.3) software at a Pt working electrode, combined with Ag/AgCl/3 mol/L KCl and a platinum wire as a reference and counter electrode, respectively. As the proposed potential modulation is not provided as ready-to-use mode in the NOVA software, an appropriate protocol was designed in the frame of a multistep chronoamperometric experiment.

## 4. Results and discussion

### 4.1 Reversible electrode reaction

A typical dimensionless response of a reversible electrode reaction is depicted in Fig. 2, revealing a wealth of electrochemical data collected in a single DSW voltammetric experiment. By analogy to the conventional SWV, the response consists of a net component ( $\Psi_{net}$ , Fig. 2A) calculated as a difference between the SW forward ( $\Psi_f$ ) and reverse ( $\Psi_r$ ) currents measured at the end of corresponding potential pulses (Fig. 2B). The technique enables measuring the current at the end of the potential step ( $\tau_s$ ) as well, thus resulting in the step component  $\Psi_s$ , which finds its analogy to the simple staircase voltammetry<sup>44</sup> (Fig. 2A). The most typical voltammetric curves of the technique are the differential forward ( $\Psi_{f,diff} = \Psi_f - \Psi_s$ ) and reverse ( $\Psi_{r,diff} = \Psi_r - \Psi_s$ )

components, calculated as a difference between the current at the end of the corresponding pulse and the step potential, following a methodology which is typical for DPV<sup>45</sup> (Fig. 2B) Note that the net component can be also defined as  $\Psi_{\text{net}} = \Psi_{\text{f,diff}} - \Psi_{\text{r,diff}}$ . Finally, an additive voltammetric component can be constructed  $\Psi_{\text{add}} = \Psi_{\text{f,diff}} + \Psi_{\text{r,diff}} = \Psi_{\text{f}} + \Psi_{\text{r}} - 2\Psi_{\text{s}}$ , which could be understood as a primitive derivation of the net voltammetric curve for a purpose of its advanced morphological characterization<sup>14</sup> (Fig. 2A).

As in SWV<sup>46</sup>, the dimensionless net peak-current ( $\Psi_{\text{net,p}}$ ) is independent on the frequency, thus the real net peak-current ( $I_{\text{net,p}}$ ) depends linearly on  $\sqrt{f}$ , for a given value of the step-to-pulse ratio ( $r$ ). In other words, the ratio  $I_{\text{net,p}}/\sqrt{f}$  is a constant for a reversible electrode reaction. As shown in Table 1, an increase of the ratio  $r$  by extending the step duration  $\tau_{\text{s}}$  for a given frequency has negligible effect on the  $\Psi_{\text{net,p}}$  over the interval  $r \leq 40$ . Thus, taking into account the current normalization, the real net peak-current can be expressed as  $I_{\text{net,p}} = (0.431 \pm 0.001) nFAc \cdot \sqrt{Df}$  for  $r \leq 40$  and conditions valid for Table 1. The later indicates that analytical performances of the technique are not sacrificed by increasing the duration of the potential steps, for the purpose of optimizing the voltammetric response in analytical application of the technique. On the contrary, the extension of  $\tau_{\text{s}}$  is expected to be beneficial for discriminating against the background parasitic current, thus improving the analytical performances.

The net peak-potential ( $E_{\text{p}}$ ) and the half-peak width are independent on the frequency, identical as in conventional SWV<sup>46</sup>, whereas, forward ( $\Psi_{\text{f}}$ ) and reverse ( $\Psi_{\text{r}}$ ) components gain more pronounced peak-like shape than in SWV (cf. Fig. 2B). It is a consequence of the overall scan rate decreasing in DSWV ( $v = \frac{2f\Delta E}{r+2}$ ) in comparison to SWV ( $v = f\Delta E$ )<sup>47</sup> for an identical frequency, causing expansion of the diffusion layer thickness in the course of the DSWV experiment. The relative position of  $\Psi_{\text{f}}$  and  $\Psi_{\text{r}}$  expressed as a peak-potential difference ( $\Delta E_{\text{p}}$ ) is independent on the frequency, whereas it is slightly affected by increasing  $r$  (cf. Table 1); e.g.,  $\Delta E_{\text{p}} = 0$  V for  $nE_{\text{sw}} = 25$  mV and  $r \leq 10$ .

The dimensionless peak-current of the step voltammetric component ( $\Psi_{\text{s,p}}$ ) is also independent on the frequency for a given value of the ratio  $r$  (Table 1), thus the



real peak-current is a linear function of  $\sqrt{f}$ . If the step-to-pulse ratio increases by extending the step potential  $\tau_s$  for a constant  $f$ , the real peak-current of the step voltammetric component increases in proportion to  $\tau_s^{-0.45}$ , which deviates slightly from the dependence of  $\tau_s^{-0.5}$ , typical for the simple staircase voltammetry<sup>44</sup>. It is expected consequence due to the complex influence of the SW potential pulses separating two consecutive step potentials. The peak potential of the step component ( $E_{s,p}$ ) is independent on both frequency and step duration; importantly it is separated for 35 mV from the net peak-potential for the conditions referring to Table 1.

Differential forward ( $\Psi_{f,diff}$ ) and reverse ( $\Psi_{r,diff}$ ) voltammetric components are unique features of the technique, providing a new means for characterization of an electrode reaction. Both components are well defined peaks, with readily and precisely measurable peak-current and peak-potential. Their relative relation represented by the peak-current ratio ( $\Psi_p(f,diff)/\Psi_p(r,diff)$ ) and the peak-potential difference ( $\Delta E_p(diff)$ ) (both parameters taken in absolute values) enable to establish new criteria for characterizing the electrode reaction. The values of  $\Psi_p(f,diff)/\Psi_p(r,diff)$  and  $\Delta E_p(diff)$  listed in Table 1 are typical for a given  $r$ , being independent on the SW frequency. Importantly, differential components enable the electrode reaction to be studied at very small SW amplitudes, as they are well defined peaks for any amplitude values over the interval  $E_{sw} \geq 2$  mV. Such analysis might be advantageous in terms of the undesirable effect of both ohmic drop and charging current, which increases proportionally to the SW amplitude in SWV<sup>48</sup>.

The effect of the SW amplitude in the present technique could be effectively studied by inspecting the peak-potential difference of differential components. Specifically,  $\Delta E_p(diff)$  vs.  $E_{sw}$  is a line with a slope equal to unity and an intercept of  $-\Delta E$ , where  $\Delta E$  is the step of the potential modulation (cf. Fig. 1B). For instance, for  $r = 10$  and  $\Delta E = 5$  mV, the corresponding linear function over the interval  $E_{sw} \leq 50$  mV reads:  $\Delta E_p(diff) \text{ (mV)} = E_{sw} \text{ (mV)} - 5 \text{ mV}$ . Both the slope and the intercept of the function are independent on the SW frequency and  $r$ , as well as on the number of electrons (specifically,  $n = 1$  or  $n = 2$ ).

At the end of this section, it is worth mentioning that the characteristics of the additive components are very specific for given conditions, and can be taken into

consideration for qualitative characterization of a reversible electrode reaction (cf. Fig. 2A). The morphology of the additive component is insensitive to the SW frequency, whereas it is highly susceptible to the SW amplitude and the number of electrons. The additive component is associated with the forward ( $\psi_p(f, \text{add})$ ) and reverse ( $\psi_p(r, \text{add})$ ) peak-current, and the potential at zero current ( $E(\psi_{\text{add}} = 0)$ ), i.e., the potential at the crossing point of the potential axis (cf. Fig. 2A). Table 1 provides values of  $E(\psi_{\text{add}} = 0)$  and the peak-current ratio ( $\psi_p(f, \text{add})/\psi_p(r, \text{add})$ ) for different values of  $r$ . For  $r \geq 10$ , the peak-current ratio is virtually independent on both time parameters  $f$  and  $r$ . In addition, the stoichiometric number of electrons can be precisely determined from the features of this voltammetric component. For instance, for simulations conducted at  $r = 4$ ,  $E_{\text{sw}} = 25$  mV,  $\Delta E = 2$  mV and  $n = 1$ , the forward-to-reverse peak-current ratio is 0.20 and  $E(\psi_{\text{add}} = 0) = -24$  mV vs.  $E^{\circ'}$ , whereas for  $n = 2$  the peak-current ratio is 0.442 and  $E(\psi_{\text{add}} = 0) = -7$  mV vs.  $E^{\circ'}$ .

#### 4.2 Quasireversible electrode reaction

The voltammetric response of a typical kinetically controlled electrode reaction under conditions of DSWV is depicted in Fig. 3. Depending on the standard rate constant ( $k_s$ ) all voltammetric curves are drifted away from the formal potential, as expected for any voltammetric technique. The relative difference between the peak-current of the net ( $\psi_{\text{net,p}}$ ) and the step component ( $\psi_{s,p}$ ) is less than for a reversible reaction (compare Fig. 2A and 3A). The morphology of the forward ( $\psi_f$ ) and reverse ( $\psi_r$ ) SW components reflects the quasireversible nature of the reaction, in analogy to the conventional SWV (cf. Fig. 3B).

As elaborated in our previous study<sup>41</sup>, main features of the dimensionless response depend on the SW frequency, manifested through the electrode kinetic parameter  $\kappa = \frac{k_s}{\sqrt{Df}}$ , which controls predominantly the degree of electrochemical reversibility. In contrast to the reversible reaction, the real net-peak-current ( $I_{\text{net,p}}$ ) is nonlinear function of  $\sqrt{f}$  for a given value of the step-to-pulse ratio (Fig. 4A). Over a broad range of frequencies, the ratio  $\frac{I_{\text{net,p}}}{\sqrt{f}}$  is not constant, obeying a sigmoid

dependence on the logarithm of  $\frac{1}{\sqrt{f}}$ . Additionally, the real peak-current of the step function depends on the SW frequency in a similar manner as the net peak-current (vide infra).

In order to generalize the effect of the frequency, it is recommendable to inspect the relation of the dimensionless peak-current of both net and step components as a function of the electrode kinetic parameter  $\kappa$ . The simulated data summarized in Fig. 4B correspond to the variation of the frequency for a constant value of both  $r$  and standard rate constant  $k_s$  over the entire kinetic interval, including irreversible, quasireversible and reversible electrochemical regions. Alternatively, the data of Fig. 4B can be understood as a comparison of a series of electrode reactions associated with different standard rate constants at a given set of time parameters, thus being associated with different electrochemical reversibility. The data clearly indicate that the net component is markedly more sensitive to the electrode kinetics than the step component. When the electrochemical reversibility is estimated on the basis of the net peak-current the data of Fig. 4B imply that the electrochemical reversibility is virtually independent on  $r$  and  $\kappa$  is the sole parameter controlling the reversibility. Within the typical quasireversible kinetic region (e.g.,  $-1.6 < \log(\kappa) < 0.8$ , for the conditions of Fig. 4B) a narrow region exists where the ratio  $I_{\text{net,p}}/\sqrt{f}$  depends linearly on  $\log(1/\sqrt{f})$  (i.e.  $-0.5 \leq \log(\kappa) \leq 0$ ), which can be used for measuring the electrode kinetics by fitting the experimental and theoretical data. Though the step peak-current follows similar sigmoid dependence on  $\log(\kappa)$ , it is markedly less sensitive than the net peak-current; moreover, for  $r \geq 20$  it is virtually independent on the SW frequency (curve **c**, circles, in Fig. 4B).

Particularly useful approach in measuring the electrode kinetics is by inspecting the peak-current ratio of the differential components ( $\Psi_p(f,\text{diff})/\Psi_p(r,\text{diff})$ ) by altering the SW frequency. As explained in our previous study<sup>41</sup>, the ratio follows a sigmoid, decreasing trend by increasing  $\log(\kappa)$ . Importantly the ratio gains the value  $\Psi_p(f,\text{diff})/\Psi_p(r,\text{diff}) = 1$  for a given critical value of the electrode kinetic parameter  $\kappa_c$ . This feature leads straightforwardly to the standard rate constant, which can be calculated as  $k_s = \kappa_c \sqrt{f_c D}$ , where  $f_c$  is the critical frequency determined experimentally, satisfying the condition  $I_p(f,\text{diff})/I_p(r,\text{diff}) = 1$ . For  $r > 2$  the critical value of  $\kappa_c$  is

independent on  $r$ , whereas it depends on the SW amplitude and the electron transfer coefficient. The critical values of  $\kappa_c$  for  $E_{sw} = 25$  mV and several values of the electron transfer coefficient are listed in Table 2. In addition, differential components can be also exploited for estimating the electrode kinetics by altering the SW amplitude and measuring the peak-potential difference ( $\Delta E_p(\text{diff})$ ). Similar to the reversible electrode reaction,  $\Delta E_p(\text{diff})$  is a linear function of  $E_{sw}$  over the interval  $E_{sw} \leq 50$  mV. However, for the quasireversible electrode reaction the slope and the intercept of the line are sensitive to both electrode kinetic parameter and the electron transfer coefficient, thus enabling estimation of  $k_s$  and  $\alpha$  by fitting of the experimental and theoretical data.

Analyzing voltammetric features at a constant frequency of the pulses by increasing the step-to-pulse ratio one finds that the ratio affects parameters of the response (Table 3). For instance, for a typical quasireversible reaction attributed with  $\log(\kappa) = -0.5$  the peak-potential difference ( $\Delta E_p$ ) between the forward and reverse SW component decreases by increasing  $r$ , opposite to the reversible reaction. If the electrochemical reversibility is estimated based on the interrelation between the forward and backward SW components ( $\Psi_p(f, \text{diff})/\Psi_p(r, \text{diff})$ ), the increasing of  $r$  shifts the electrode reaction toward higher electrochemical reversibility, as already discussed in our previous study<sup>41</sup>. As a consequence, the quasireversible region of a sluggish electrode reaction is expanded by increasing  $r$ , as seen in Fig. 4B (triangles; the kinetic region which is near the irreversible behavior).

For a constant frequency, within the quasireversible region, the real step peak-current decreases with  $\tau_s^{-0.4}$ , which is slightly different compared to the reversible reaction. At the same time, the peak potentials of both net and step components shifts toward less potentials as a consequence of a decreased scan rate, thus an enhanced electrochemical reversibility (cf. Table 3).

It is finally worth mentioning that the additive component is particularly sensitive to the electrode kinetics and can be effectively exploited for a precise estimation of the kinetic parameters<sup>22</sup>. Figure 5 depicts the additive component for different degree of reversibility, showing that both peak-current ratio ( $\Psi_p(f, \text{add})/\Psi_p(r, \text{add})$ ) and the crossing point at the potential axis ( $E(\Psi_{\text{add}} = 0)$ ) vary significantly with the electrode kinetic parameter. By extensive simulations under a variety of conditions it has been

determined that the highest measurable values of the standard rate constant by means of the features of the additive component are in order of  $0.1 \text{ cm s}^{-1}$ .

## 5. Experimental data

A well-defined voltammetric response of the redox couple  $\text{Fe}(\text{CN})_6^{3-}/[\text{Fe}(\text{CN})_6]^{4-}$  at a platinum electrode, measured for the step-to-pulse duration ratio  $r = 5$ , and the SW frequency of  $f = 8$ , illustrates experimentally the applicability of the technique (Fig. 6). In spite of the well-known complexity of the electrode reaction of hexacyanoferrates<sup>49-52</sup>, the features of the voltammetric response under selected experimental conditions correspond to the theoretical predictions for a fast, quasireversible electrode reaction<sup>42</sup>.

The richness of the voltammetric data collected in a single experiment enable effective characterization of the studied system, which is one of the advantages of the proposed technique. For instance, analyzing the voltammetric data in Fig. 6A one finds that the crossing point at the potential axis of the additive component is  $E(I_{\text{add}} = 0) = -15 \text{ mV vs. } E^0$ , whereas the peak potential of the step component is  $E_{\text{s,p}} = 40 \text{ mV vs. } E^0$ . Here we assume that  $E^0$  is identical with the net peak-potential. The peak-current ratio of the net and the step component is  $I_{\text{net,p}}/I_{\text{s,p}} = 7.03$ , while the ratio of the forward and backward peaks of the additive component is  $I_{\text{p}}(\text{f,add})/I_{\text{p}}(\text{r,add}) = 0.481$ .

Conducting simulations under corresponding conditions, by assuming a fast electrode reaction with  $\log(\kappa) = 0.13$  ( $\alpha = 0.5$  and  $n = 1$ )<sup>46</sup>, one finds that  $E(\Psi_{\text{add}} = 0) = -15 \text{ mV vs. } E^0$  and  $E_{\text{s,p}} = 40 \text{ mV vs. } E^0$ , whereas the peak-current ratios are  $\Psi_{\text{net,p}}/\Psi_{\text{s,p}} = 7.61$  and  $\Psi_{\text{p}}(\text{f,add})/\Psi_{\text{p}}(\text{r,add}) = 0.484$ , which is in excellent agreement with the experimental data. Let us note that if the simulations are done with the stoichiometric number of electrons  $n = 2$  the ratio is  $\Psi_{\text{p}}(\text{f,add})/\Psi_{\text{p}}(\text{r,add}) = 0.651$ , which does not correspond to experimental value. Hence, as indicated in the theoretical part, the ratio  $\Psi_{\text{p}}(\text{f,add})/\Psi_{\text{p}}(\text{r,add})$  can be effectively exploited for estimation of the number of electrons in the electrode equation.

Referring to the forward and backward components presented in Fig. 6B, the peak potentials separation ( $\Delta E_{\text{p}}$ ) of the SW components is close to  $25 \text{ mV}$ , while the differential components are separated for  $45 \text{ mV}$  ( $\Delta E_{\text{p}}(\text{diff})$ ). The peak-current ratio of

the differential components is  $I_p(f,diff)/I_p(r,diff) = 0.872$ . Theoretical data simulated for  $\log(\kappa) = 0.13$  are associated with potential separation of 30 and 45 mV for the SW and differential components, respectively, whereas the peak-current ratio is  $\Psi_p(f,diff)/\Psi_p(r,diff) = 0.810$ .

Further experimental analysis has been done by changing the step-to-pulse duration ratio  $r$  within the interval from 1 to 25, for a constant SW frequency of  $f = 8\text{ Hz}$ . As predicted by the theory for reversible or fast electrode reaction the peak-potential of both net and step components remained unaffected by  $r$  (cf. Table 1). The net peak-current slightly varied with  $r$ , with an average value of  $I_{\text{net,p}} = (7.78 \pm 0.23) \mu\text{A}$ , whereas the peak-current of the step component is a linear function of  $r^{-0.45}$  ( $R^2 = 0.999$ ), which is in excellent agreement with the theoretical predictions. The peak-current ratio of the differential forward and reverse components increases from 0.73 to 0.85 for  $r = 1$  and 25 respectively; the same trend holds for the peak-current ratio of the additive components, which is in agreement with the data in Table 1.

Finally, the effect of the SW amplitude was studied for three values of  $r$  (i.e.,  $r = 1, 5$  and  $10$ ) and the peak-potential separation ( $\Delta E_p(\text{diff})$ ) of the differential forward and backward components was measured as a function of  $E_{\text{sw}}$  over the amplitude interval from 5 to 50 mV. Generally, the relationship  $\Delta E_p(\text{diff})$  vs.  $E_{\text{sw}}$  does not depend on  $r$ , as predicted by the simulations for a reversible reaction. The best linearity was found for  $r = 5$ , and the regression line is  $\Delta E_p(\text{diff}) = 0.967E_{\text{sw}} + 4.70$  ( $R^2 = 0.905$ ), where all values are expressed in millivolts. These experimental data are in accord with the theory in which it was predicted that the intercept of the latter function is 1, while the slope is equal to the step potential increment (i.e., 5 mV in the present experiment).

## 6. Conclusions

Differential square-wave voltammetry is a novel, hybrid technique between conventional differential pulse and square-wave voltammetry, which is designed to unify the advantages of both techniques, in terms of analytical sensitivity, mechanistic and kinetic characterization of both very fast and sluggish electrode processes. A single voltammogram consists of seven voltammetric curves; hence, a plethora of voltammetric parameters can be measured (i.e., peak-currents and peak-potentials),

in addition to the interrelation between these parameters (i.e., peak-current ratios and peak-potential differences), providing a basis for effective and in-depth characterization of the studied electrode reaction in a fast and effective procedure. In addition, the additive voltammetric component provides a new means for estimation of number of electrons in the electrode reaction equation, electron transfer coefficient and the standard rate constant, extending the kinetic interval up to rate constants of  $0.1 \text{ cm}^2 \text{ s}^{-1}$ . The nature of differential and additive voltammetric components do not require background corrections in the experimental analysis, thus providing voltammetric data of superior quality, which leads to a reliable kinetic characterization as well as promising advanced analytical application of the technique.

## Acknowledgement

VM and DG are grateful for the support of the Opus Lap grant no. 2020/39/I/ST4/01854 by the National Science Centre of Poland.

## References

1. Batchelor-McAuley, C.; Kätelhön, E.; Barnes, E. O.; Compton, R. G.; Laborda, E.; Molina, A., Recent Advances in Voltammetry. *ChemistryOpen* **2015**, *4* (3), 224-260.
2. Laborda, E.; González, J.; Molina, Á., Recent advances on the theory of pulse techniques: A mini review. *Electrochemistry Communications* **2014**, *43*, 25-30.
3. Laborda, E.; Martínez-Ortiz, F.; Molina, Á., Study of Electrochemical Processes with Coupled Homogeneous Chemical Reaction in Differential Pulse Voltammetry at Spherical Electrodes and Microhemispheres. *Electroanalysis* **2010**, *22* (16), 1857-1866.
4. Molina, A.; González, J.; Laborda, E.; Wang, Y.; Compton, R. G., Catalytic mechanism in cyclic voltammetry at disc electrodes: an analytical solution. *Phys Chem Chem Phys* **2011**, *13* (32), 14694-14704.
5. Molina, A.; Gonzalez, J.; Laborda, E.; Li, Q.; Batchelor-McAuley, C.; Compton, R. G., Electrochemical Behavior of Two-Electron Redox Processes by Differential Pulse

- Techniques at Microelectrodes. *The Journal of Physical Chemistry C* **2012**, *116* (1), 1070-1079.
6. Rudolph, M., Digital simulation with the fast implicit finite difference (FIFD) algorithm: Part 5: Digital simulations of square wave voltammetry for any user defined electrochemical mechanism comprising first- and second-order chemical reactions. *Journal of Electroanalytical Chemistry* **2001**, *503* (1), 15-27.
7. Dickinson, E. J. F.; Ekström, H.; Fontes, E., COMSOL Multiphysics®: Finite element software for electrochemical analysis. A mini-review. *Electrochemistry Communications* **2014**, *40*, 71-74.
8. Britz, D.; Strutwolf, J., *Digital Simulation in Electrochemistry*. 2016.
9. Mirčeski, V.; Lovrić, M., Split square-wave voltammograms of surface redox reactions. *Electroanalysis* **1997**, *9* (16), 1283-1287.
10. Mirceski, V.; Guziejewski, D.; Lisichkov, K., Electrode kinetic measurements with square-wave voltammetry at a constant scan rate. *Electrochimica Acta* **2013**, *114*, 667-673.
11. Guziejewski, D.; Mirceski, V.; Jadresko, D., Measuring the Electrode Kinetics of Surface Confined Electrode Reactions at a Constant Scan Rate. *Electroanalysis* **2015**, *27* (1), 67-73.
12. Mirceski, V.; Smarzewska, S.; Guziejewski, D., Measuring the Electrode Kinetics of Vitamin B2 at a Constant Time Window of a Square Wave Voltammetric Experiment. *Electroanalysis* **2016**, *28* (2), 385-393.
13. Mirceski, V.; Laborda, E.; Guziejewski, D.; Compton, R. G., New Approach to Electrode Kinetic Measurements in Square-Wave Voltammetry: Amplitude-Based Quasireversible Maximum. *Analytical Chemistry* **2013**, *85* (11), 5586-5594.
14. Molina, A.; González, J., *Pulse Voltammetry in Physical Electrochemistry and Electroanalysis Theory and Applications*. 1st ed. 2016. ed.; 2016.
15. Dauphin-Ducharme, P.; Arroyo-Currás, N.; Kurnik, M.; Ortega, G.; Li, H.; Plaxco, K. W., Simulation-Based Approach to Determining Electron Transfer Rates Using Square-Wave Voltammetry. *Langmuir* **2017**, *33* (18), 4407-4413.
16. Gulaboski, R.; Mirceski, V., New aspects of the electrochemical-catalytic (EC') mechanism in square-wave voltammetry. *Electrochimica Acta* **2015**, *167*, 219-225.
17. Lovrić, M.; Komorsky-Lovric, Š., Square-wave voltammetry of an adsorbed reactant. *Journal of Electroanalytical Chemistry and Interfacial Electrochemistry* **1988**, *248* (2), 239-253.



18. Laborda, E.; Henstridge, M. C.; Molina, A.; Martínez-Ortiz, F.; Compton, R. G., A comparison of Marcus–Hush vs. Butler–Volmer electrode kinetics using potential pulse voltammetric techniques. *Journal of Electroanalytical Chemistry* **2011**, *660* (1), 169-177.
19. Laborda, E.; Wang, Y.; Henstridge, M. C.; Martínez-Ortiz, F.; Molina, A.; Compton, R. G., Quantitative weaknesses of the Marcus-Hush theory of electrode kinetics revealed by Reverse Scan Square Wave Voltammetry: The reduction of 2-methyl-2-nitropropane at mercury microelectrodes. *Chemical Physics Letters* **2011**, *512* (1), 133-137.
20. Laborda, E.; Henstridge, M. C.; Compton, R. G., Asymmetric Marcus theory: Application to electrode kinetics. *Journal of Electroanalytical Chemistry* **2012**, *667*, 48-53.
21. Molina, A.; Laborda, E.; Martínez-Ortiz, F.; Bradley, D. F.; Schiffrin, D. J.; Compton, R. G., Comparison between double pulse and multipulse differential techniques. *Journal of Electroanalytical Chemistry* **2011**, *659* (1), 12-24.
22. Molina, A.; Moreno, M. M.; Serna, C.; Camacho, L., Additive differential pulse voltammetry, instead of double differential pulse voltammetry. *Electrochemistry Communications* **2001**, *3* (7), 324-329.
23. Stoytcheva, M.; Zlatev, R.; Velkova, Z.; Gochev, V.; Ayala, A.; Montero, G.; Valdez, B., Resolution of a Mononitrophenol Isomers Mixture by Differential Alternative Pulses Voltammetry. *Electroanalysis* **2019**, *31* (4), 652-660.
24. Zlatev, R.; Stoytcheva, M.; Valdez, B., Application of Anodic Stripping Differential Alternative Pulses Voltammetry for Simultaneous Species Quantification. *Electroanalysis* **2018**, *30* (9), 1902-1905.
25. Ayala, A.; Stoytcheva, M.; Zlatev, R.; Velkova, Z.; Gochev, V.; Valdez, B.; Montero, G., Simultaneous Determination of Hydroquinone and Catechol by Differential Alternative Pulses Voltammetry. *Electroanalysis* **2018**, *30* (9), 1913-1917.
26. Jadreško, D.; Zelić, M., Cyclic multipulse voltammetric techniques. Part I: Kinetics of electrode processes. *Journal of Electroanalytical Chemistry* **2013**, *707*, 20-30.
27. Lovrić, M.; Jadreško, D., Theory of square-wave voltammetry of quasireversible electrode reactions using an inverse scan direction. *Electrochimica Acta* **2010**, *55* (3), 948-951.
28. Zelić, M.; Lovrić, M., Isopotential points in reverse square-wave voltammetry. *Journal of Electroanalytical Chemistry* **2009**, *637* (1), 28-32.

29. Xinsheng, C.; Guogang, P., Cyclic Square Wave Voltammetry: Theory and Experimental. *Analytical Letters* **1987**, *20* (10), 1511-1519.
30. Helfrick Jr., J. C.; Mann, M. A.; Bottomley, L. A., Diagnostic Criteria for the Characterization of Electrode Reactions with Chemically Coupled Reactions Preceding the Electron Transfer by Cyclic Square Wave Voltammetry. *ChemPhysChem* **2016**, *17* (16), 2596-2606.
31. Helfrick, J. C.; Bottomley, L. A., Cyclic Square Wave Voltammetry of Single and Consecutive Reversible Electron Transfer Reactions. *Analytical Chemistry* **2009**, *81* (21), 9041-9047.
32. Kätelhön, E.; Compton, R. G., Non-linear sweep voltammetry of adsorbed species: theory and a method to determine formal potentials. *Phys Chem Chem Phys* **2017**, *19* (42), 28820-28823.
33. Uchida, Y.; Kätelhön, E.; Compton, R. G., Cyclic voltammetry with non-triangular waveforms: Electrochemically irreversible and quasi-reversible systems. *Journal of Electroanalytical Chemistry* **2018**, *810*, 135-144.
34. Stojanov, L.; Guziejewski, D.; Puiu, M.; Bala, C.; Mirceski, V., Multi-frequency analysis in a single square-wave chronoamperometric experiment. *Electrochemistry Communications* **2021**, *124*.
35. Jadreško, D.; Guziejewski, D.; Mirčeski, V., Electrochemical Faradaic Spectroscopy. *ChemElectroChem* **2018**, *5* (1), 187-194.
36. Mirceski, V.; Gulaboski, R.; Lovric, M.; Bogeski, I.; Kappl, R.; Hoth, M., Square-Wave Voltammetry: A Review on the Recent Progress. *Electroanalysis* **2013**, *25* (11), 2411-2422.
37. Mirceski, V.; Gulaboski, R., Recent Achievements in Square-Wave Voltammetry (a Review). *Maced J Chem Chem En* **2014**, *33* (1), 1-12.
38. Mirceski, V.; Stojanov, L.; Gulaboski, R., Double-sampled differential square-wave voltammetry. *Journal of Electroanalytical Chemistry* **2020**, *872*.
39. Chen, A.; Shah, B., Electrochemical sensing and biosensing based on square wave voltammetry. *Analytical Methods* **2013**, *5* (9), 2158-2173.
40. Castagnola, E.; Woepel, K.; Golabchi, A.; McGuier, M.; Chodapaneedi, N.; Metro, J.; Taylor, I. M.; Cui, X. T., Electrochemical detection of exogenously administered melatonin in the brain. *Analyst* **2020**, *145* (7), 2612-2620.
41. Mirceski, V.; Guziejewski, D.; Stojanov, L.; Gulaboski, R., Differential Square-Wave Voltammetry. *Analytical Chemistry* **2019**, *91* (23), 14904-14910.

42. Daum, P. H.; Enke, C. G., Electrochemical kinetics of the ferri-ferrocyanide couple on platinum. *Analytical Chemistry* **1969**, *41* (4), 653-656.
43. Nicholson, R. S.; Olmstead, M. L., Electrochemistry: calculations, simulation, and instrumentation. Mattson, J. S.; Mark, H. B.; MacDonald, H. C., Eds. New York : M. Dekker: New York, 1972; pp 120-137.
44. Christie, J. H.; Lingane, P. J., Theory of staircase voltammetry. *Journal of Electroanalytical Chemistry (1959)* **1965**, *10* (3), 176-182.
45. Barker, G. C.; Gardner, A. W., Pulse polarography. *Fresenius' Zeitschrift für analytische Chemie* **1960**, *173* (1), 79-83.
46. Mirceski, V.; Komorsky-Lovric, S.; Lovric, M., *Square-Wave Voltammetry: Theory and Application*. Springer Berlin Heidelberg: 2007.
47. Jadreško, D.; Zelić, M.; Lovrić, M., A formal scan rate in staircase and square-wave voltammetry. *Journal of Electroanalytical Chemistry* **2010**, *645* (2), 103-108.
48. Krulic, D.; Fatouros, N., Peak heights and peak widths at half-height in square wave voltammetry without and with ohmic potential drop for reversible and irreversible systems. *Journal of Electroanalytical Chemistry* **2011**, *652* (1), 26-31.
49. Peter, L. M.; Dürr, W.; Bindra, P.; Gerischer, H., The influence of alkali metal cations on the rate of the  $\text{Fe}(\text{CN})_6^{4-}/\text{Fe}(\text{CN})_6^{3-}$  electrode process. *Journal of Electroanalytical Chemistry and Interfacial Electrochemistry* **1976**, *71* (1), 31-50.
50. Bindra, P.; Gerischer, H.; Peter, L. M., The dependence of the rate of the  $\text{Fe}(\text{CN})_6^{3-}/\text{Fe}(\text{CN})_6^{4-}$  couple on ionic strength in concentrated solutions. *Journal of Electroanalytical Chemistry and Interfacial Electrochemistry* **1974**, *57* (3), 435-438.
51. Kim, D. Y.; Wang, J.; Yang, J.; Kim, H. W.; Swain, G. M., Electrolyte and Temperature Effects on the Electron Transfer Kinetics of  $\text{Fe}(\text{CN})_6^{3-/4-}$  at Boron-Doped Diamond Thin Film Electrodes. *The Journal of Physical Chemistry C* **2011**, *115* (20), 10026-10032.
52. Noel, M.; Anantharaman, P. N., Voltammetric studies on a glassy carbon electrode. Part II. Factors influencing the simple electron-transfer reactions—the  $\text{K}_3[\text{Fe}(\text{CN})_6]$ - $\text{K}_4[\text{Fe}(\text{CN})_6]$  system. *Analyst* **1985**, *110* (9), 1095-1103.

## Figures and figure captions

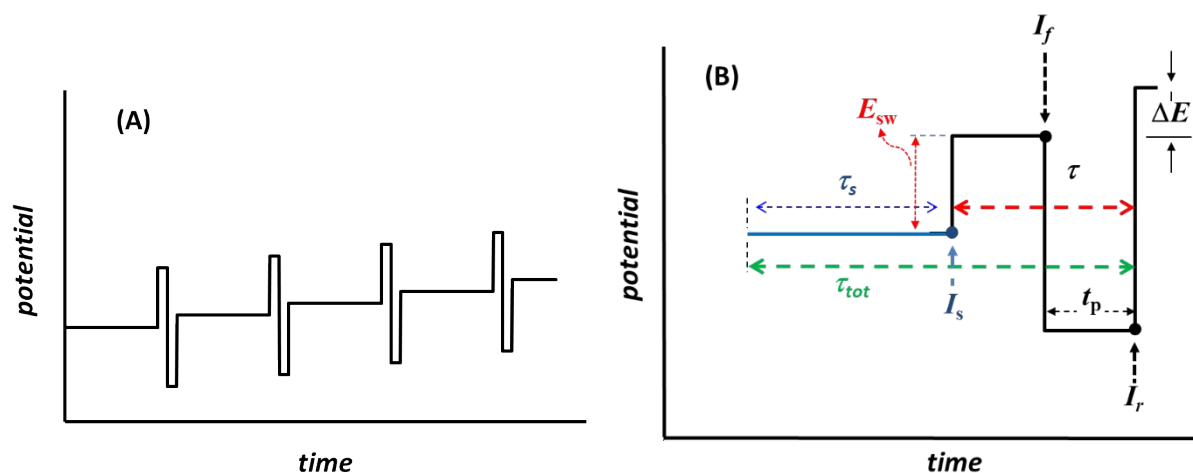


**Figure 1.** (A) Potential modulation and (B) one single potential cycle in differential square-wave voltammetry. Panel B shows critical parameters of the potential modulation together with the current sampling points.

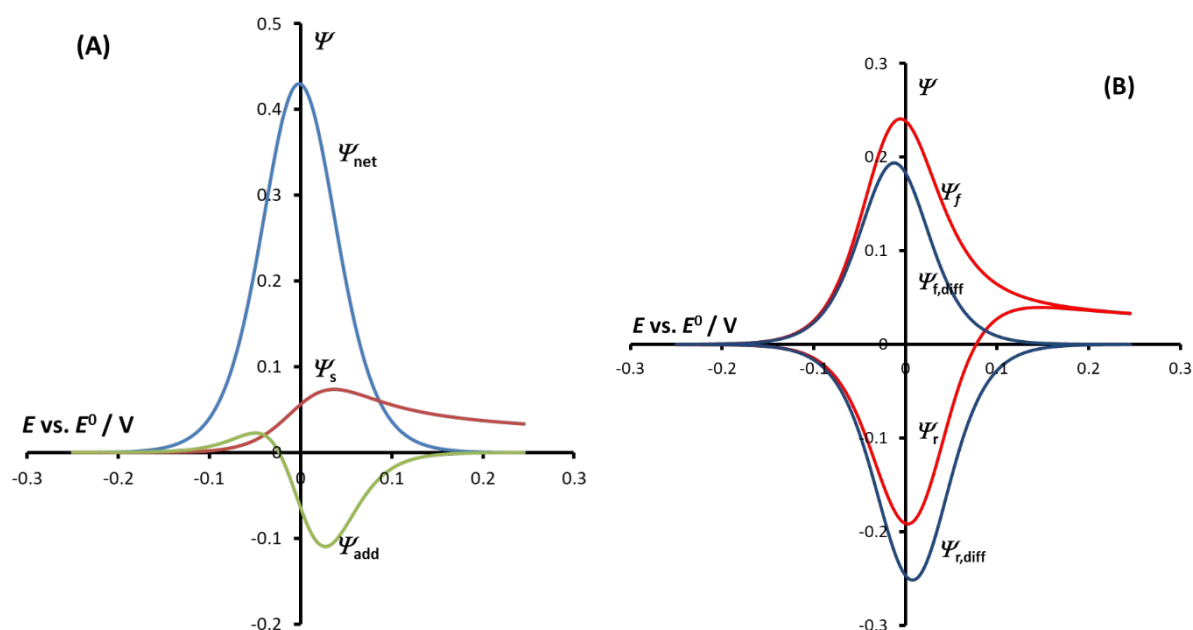


**Figure 2.** Reversible electrode reaction. Typical response showing all voltammetric components for the step-to-pulse ratio  $r = 10$ . Panel (A) depicts the net component ( $\Psi_{net}$ ), the step component ( $\Psi_s$ ) and the additive component ( $\Psi_{add}$ ), while panel (B) displays the square-wave forward ( $\Psi_f$ ) and reverse ( $\Psi_r$ ) components, and the differential forward ( $\Psi_{f,diff}$ ) and reverse ( $\Psi_{r,diff}$ ) components. The conditions of the simulations are: temperature  $T = 298.15$  K, stoichiometric number of electrons  $n = 1$ , SW amplitude  $E_{sw} = 25$  mV and step potential  $\Delta E = 5$  mV.

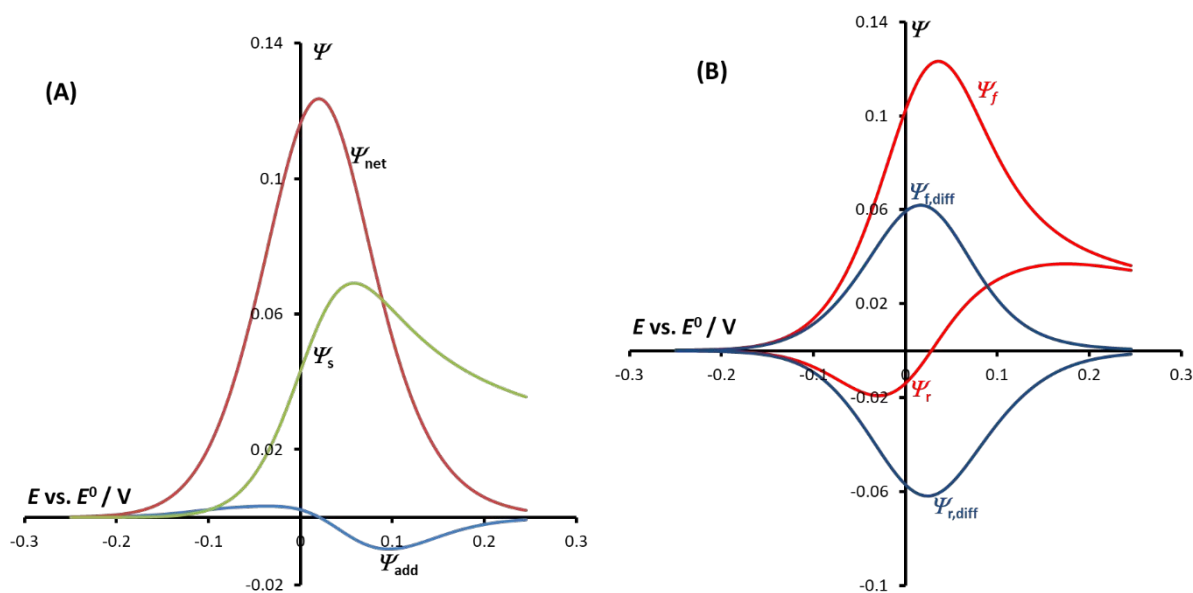


**Figure 3.** One-electron quasireversible electrode reaction. A typical response containing all voltammetric components for the standard rate constant  $k_s = 3 \times 10^{-3} \text{ cm s}^{-1}$ , electron transfer coefficient  $\alpha = 0.5$ , diffusion coefficient  $D = 5 \times 10^{-6} \text{ cm}^2 \text{ s}^{-1}$ , and SW frequency  $f = 100 \text{ Hz}$ . The other conditions and meaning of symbols are identical as in Fig. 2.

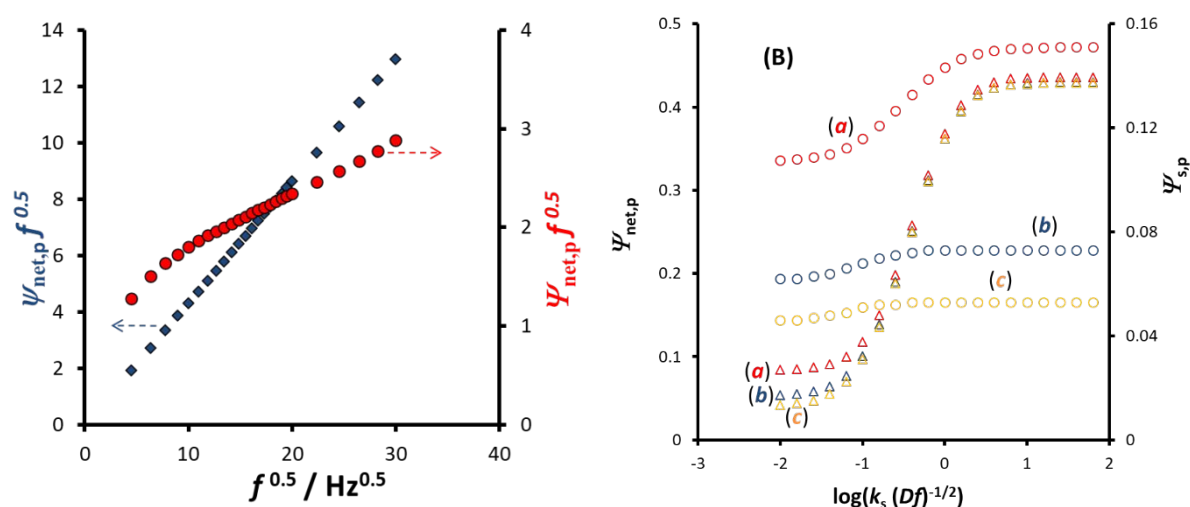


**Figure 4. (A)** The effect of the SW frequency on the normalized real net peak-current for a reversible (rhombuses, left ordinate) and a quasireversible (circles, right ordinate) electrode reaction, for step-to-pulse ratio of  $r = 4$  and the standard rate constant  $k_s = 5 \times 10^{-3} \text{ cm s}^{-1}$ . **(B)** The dependence of the dimensionless net peak-current (triangles, left ordinate) and the step peak-current (circles, right ordinate) on the electrode kinetic parameter for the step-to-pulse ratio  $r = 2$  (a); 10 (b) and 20 (c). The other conditions of the simulations are identical as in Fig. 3.

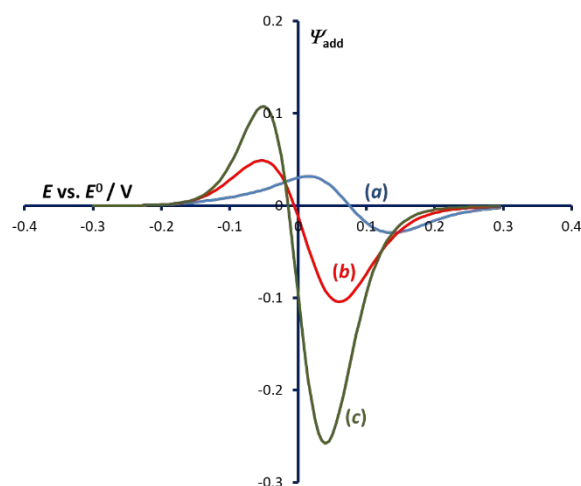


**Figure 5.** One-electron quasireversible electrode reaction. The additive voltammetric component simulated for different electrochemical reversibility. The electrode kinetic parameter is:  $\log(\kappa) = -1$  (a);  $-0.5$  (b) and  $0$  (c). The step-to-pulse ratio is  $r = 2$ , and electron transfer coefficient  $\alpha = 0.5$ . The other conditions are identical as in Fig. 2.

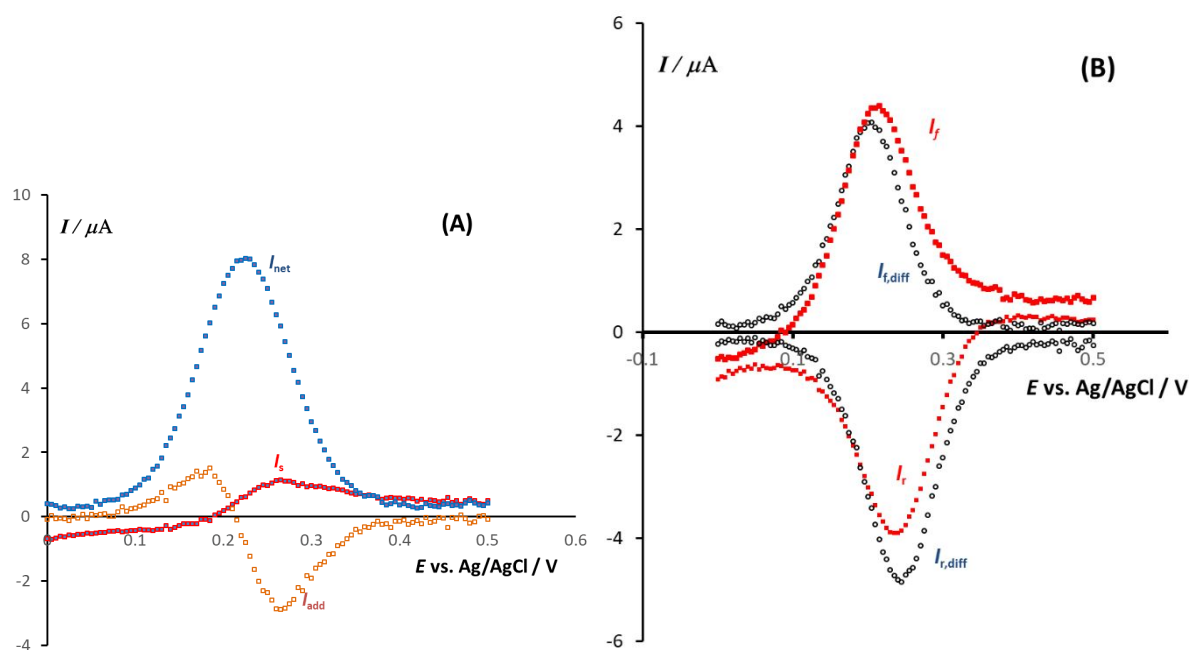


**Figure 6.** A typical experimental voltammetric response under conditions of DSUV of  $[\text{Fe}(\text{CN})_6]^{4-}/[\text{Fe}(\text{CN})_6]^{3-}$  at equimolar bulk concentration of both components of the redox couple of  $0.25 \text{ mmol/L}$ , recorded in  $0.100 \text{ mol/L}$  aqueous solution of  $\text{KNO}_3$  at Pt electrode. Panel **(A)** depicts the net ( $I_{\text{net}}$ ), the step ( $I_s$ ) and the additive ( $I_{\text{add}}$ ) voltammetric components, while panel **(B)** displays the square-wave forward ( $I_f$ ) and reverse ( $I_r$ ) components, and the differential forward ( $I_{f,\text{diff}}$ ) and reverse ( $I_{r,\text{diff}}$ ) components. The step-to-pulse ratio is  $r = 5$ . Other parameters of the potential modulation are  $f = 8 \text{ Hz}$ ,  $E_{\text{sw}} = 50 \text{ mV}$  and  $\Delta E = 5 \text{ mV}$ .

## Tables

**Table 1.** Reversible electrode reaction. Typical parameters of the DSWV response for one-electron ( $n = 1$ ) reaction as a function of the step-to pulse ratio ( $r$ ), simulated for SW amplitude  $E_{sw} = 25$  mV, step potential  $\Delta E = 5$  mV, and temperature  $T = 298.15$  K. The table lists the values of net peak-current ( $\Psi_{net,p}$ ), net peak-potential ( $E_p$ ), peak potential difference of the SW forward and reverse components ( $\Delta E_p$ ), step peak-current ( $\Psi_{s,p}$ ), step peak-potential ( $E_{s,p}$ ), the peak-current ratio in absolute values of the differential forward and reverse components ( $\Psi_p(f,diff)/\Psi_p(r,diff)$ ), their peak-potential difference ( $\Delta E_p(diff)$ ), the peak-current ratio of the additive component ( $\Psi_p(f,add)/\Psi_p(b,add)$ ) and the potential of the crossing point at the potential axis of the additive component ( $E(\Psi_{add} = 0)$ ).

$r = \tau_s/t_p$	$\Psi_{net,p}$	$E_p$ vs. $E^\circ/V$	$\Delta E_p$ /mV	$\Psi_{s,p}$	$E_{s,p}$ vs. $E^\circ/V$	$\Psi_p(f,diff)/\Psi_p(r,diff)$	$\Delta E_p(diff)$ /mV	$\Psi_p(f,add)/\Psi_p(r,add)$	$E(\Psi_{add} = 0)$ vs. $E^\circ/V$
2	0.433	0	0	0.151	0.035	0.723	20	0.118	-0.030
3	0.433	0	0	0.126	0.035	0.723	20	0.155	-0.027
4	0.432	0	0	0.111	0.035	0.742	20	0.175	-0.025
5	0.431	0	0	0.100	0.035	0.752	20	0.186	-0.025
6	0.431	0	0	0.093	0.035	0.759	20	0.193	-0.025
7	0.431	0	0	0.086	0.035	0.763	20	0.198	-0.025
8	0.430	0	0	0.081	0.035	0.766	20	0.202	-0.025
9	0.430	0	0	0.077	0.035	0.768	20	0.204	-0.025
10	0.430	0	5	0.073	0.035	0.770	20	0.207	-0.025
11	0.430	0	5	0.070	0.035	0.771	20	0.208	-0.025
12	0.430	0	5	0.067	0.035	0.772	20	0.210	-0.025
14	0.430	0	10	0.063	0.035	0.773	20	0.212	-0.025
16	0.429	0	10	0.059	0.035	0.774	20	0.213	-0.025
20	0.429	0	10	0.053	0.035	0.776	20	0.215	-0.025
40	0.429	0	15	0.038	0.035	0.778	20	0.219	-0.025

**Table 2.** One-electron quasireversible electrode reaction. Critical values of the electrode kinetic parameter  $\kappa_c$ , which satisfy the condition  $\Psi_p(f,diff)/\Psi_p(r,diff) = 1$ , calculated for  $r = 6$  and different values of the electron transfer coefficient,  $\alpha$ . All other conditions are identical as for Table 1.

$\alpha$	$\kappa_c$
0.30	0.05
0.35	0.07
0.40	0.09
0.45	0.11
0.50	0.13
0.55	0.16
0.60	0.19
0.65	0.22
0.70	0.25

**Table 3.** One-electron quasireversible electrode reaction. Typical parameters of the DSWV response as a function of the step-to pulse ratio ( $r$ ) for electrode kinetic parameter  $\log(\kappa) = -0.5$ . All other conditions and notations are identical as for Table 1.

$r = \tau_s/t_p$	$\Psi_{net,p}$	$E_p$ vs. $E^0/V$	$\Delta E_p$ /mV	$\Psi_{s,p}$	$E_{s,p}$ vs. $E^0/V$	$\frac{\Psi_p(f,diff)}{\Psi_p(r,diff)}$	$\Delta E_p(diff)$ /mV	$\frac{\Psi_p(f,add)}{\Psi_p(r,add)}$	$E(\Psi_{add} = 0)$ vs. $E^0/V$
2	0.227	0.015	50	0.130	0.050	0.805	20	0.120	-0.035
3	0.225	0.015	40	0.114	0.050	0.832	15	0.170	-0.028
4	0.223	0.010	35	0.103	0.045	0.847	15	0.201	-0.025
5	0.222	0.010	30	0.095	0.045	0.856	15	0.221	-0.023
6	0.221	0.010	30	0.089	0.045	0.862	15	0.235	-0.023
7	0.221	0.010	30	0.083	0.045	0.867	15	0.245	-0.022
8	0.220	0.010	20	0.079	0.040	0.870	15	0.252	-0.022
9	0.220	0.010	20	0.075	0.040	0.872	15	0.258	-0.021
10	0.220	0.010	20	0.072	0.040	0.873	15	0.263	-0.021
11	0.220	0.005	20	0.069	0.040	0.874	15	0.266	-0.021
12	0.219	0.005	20	0.066	0.040	0.875	15	0.269	-0.021
14	0.219	0.005	15	0.062	0.040	0.875	15	0.273	-0.021
16	0.219	0.005	10	0.058	0.035	0.876	10	0.275	-0.021
20	0.218	0.005	15	0.053	0.035	0.876	10	0.278	-0.021